

JOURNAL OF MECHANICAL ENGINEERING

An International Journal

VOLUME 13 No. 1

JUNE 2016 / ISSN 1823-5514



JOURNAL OF MECHANICAL ENGINEERING

An International Journal

EDITOR IN CHIEF:

Professor Wahyu Kuntjoro – Universiti Teknologi MARA, Malaysia

Professor Salmiah Kasolang – Universiti Teknologi MARA, Malaysia

Professor Essam E. Khalil – University of Cairo, Egypt

EDITORIAL BOARD:

Datuk Professor Ow Chee Sheng – Universiti Teknologi MARA, Malaysia

Professor Ichsan S. Putra – Bandung Institute of Technology, Indonesia

Dr. Ahmad Azlan Mat Isa – Universiti Teknologi MARA, Malaysia

Professor Shahrir Abdullah – Universiti Kebangsaan Malaysia

Dr. Faqir Gul – Institute Technology Brunei, Brunei Darussalam

Professor Shahrum Abdullah – Universiti Kebangsaan Malaysia

Dr. Mohd. Afian Omar – SIRIM Malaysia

Professor Masahiro Ohka – Nagoya University, Japan

Dr. Valliyappan David a/l Natarajan – Universiti Teknologi MARA, Malaysia

Professor Mirosław L Wyszynski – University of Birmingham, UK

Dr. Yongki Go Tiauw Hiong – Florida Institute of Technology, USA

Professor Mohamad Nor Berhan – Universiti Teknologi MARA, Malaysia

Professor Abdelmagid Salem Hamouda – Qatar University, Qatar

Professor P. N. Rao – University of Northern Iowa, USA

Professor Abdul Rahman Omar – Universiti Teknologi MARA, Malaysia

Professor Wirachman Wisnoe – Universiti Teknologi MARA, Malaysia

Professor Ahmed Jaffar – Universiti Teknologi MARA, Malaysia

Professor Yongtae Do – Daegu University, Korea

Professor Bernd Schwarze – University of Applied Science, Osnabrueck, Germany

EDITORIAL EXECUTIVES:

Professor Bodo Heimann – Leibniz University of Hannover Germany

Dr. Solehuddin Shuib

Professor Darius Gnanaraj Solomon – Karunya University, India

Dr. Muhad Rozi Mat Nawi

Professor Hazizan Md. Akil – Universiti Sains Malaysia, Malaysia

Dr. Noor Azlina Mohd Salleh

Professor Mohd. Zulkifly Abdullah – Universiti Sains Malaysia, Malaysia

Dr. Siti Mariam Abdul Rahman

Professor Roslan Abd. Rahman – Universiti Teknologi Malaysia, Malaysia

Dr. Mohd Faizal bin Mohamad

Dr. Baljit Singh A/L Bathal Singh

Nurul Hayati Abdul Halim

Rosnadiyah Bahsan

Copyright © 2016 by the Faculty of Mechanical Engineering (FKM), Universiti Teknologi MARA, 40450 Shah Alam, Selangor, Malaysia.

All rights reserved. No part of this publication may be reproduced, stored in a retrieval system, or transmitted in any form or any means, electronic, mechanical, photocopying, recording or otherwise, without prior permission, in writing, from the publisher.

Journal of Mechanical Engineering (ISSN 1823-5514) is published by the Faculty of Mechanical Engineering (FKM) and UiTM Press, Universiti Teknologi MARA, 40450 Shah Alam, Selangor, Malaysia.

The views, opinions and technical recommendations expressed herein are those of individual researchers and authors and do not necessarily reflect the views of the Faculty or the University.

JOURNAL OF MECHANICAL ENGINEERING

An International Journal

Vol. 13 No. 1	June 2016	ISSN 1823-5514
---------------	-----------	----------------

1. Analysis of Crack Propagation in an Adhesive Joint 1
M.D. Mohan Gift
J. Selvakumar
S. John Alexis

2. Analysis of the Thermal Behavior of the Double Skin Envelope 13
in the Full Scale Testing Modules of the Postgraduate Unit for a
Cloudy and a Clear Day
Ricardo Sánchez Benítez
Leonardo B. Zeevaert Alcántara

3. Energy Conversion from Biodegradation of Non-thermal Pre- 25
treated Algae Biomass for Microbial Fuel Cell
Muhammad Haikal Zainal
Oskar Hasdinor Hassan
Liana Shakira Ab Samad
Ab Malik Marwan Ali
Muhd Zu Azhan Yahya

4. Mode III Stress Intensity Factors of Sickle-Shaped Surface 33
Cracks in Round Bars
A.E Ismail

5. Perpendicular Dowel-bearing Strength Properties without Glue Line for Mengkulang Species 45
Nor Jihan Abd Malek
Rohana Hassan
Tengku Anita Raja Hussin
Ng Dick Tern
Constantine Adam
6. The Use of Edible Vertical Greenery System to Improve Thermal Performance in Tropical Climate 57
Hazril Sherney Basher
Sabarinah Sh Ahmad
Abdul Malek Abdul Rahman
Nurulhusna Qamaruz Zaman

Mode III Stress Intensity Factors of Sickle-Shaped Surface Cracks in Round Bars

A.E Ismail

*Department of Engineering Mechanics,
Faculty of Mechanical and Manufacturing Engineering,
Universiti Tun Hussein Onn Malaysia,
86400 Batu Pahat, Johor, Malaysia
E-mail: emran@uthm.edu.my / al_emran@hotmail.com*

ABSTRACT

The solutions of stress intensity factors (SIFs) of sickle-shaped surface crack in round bars are not currently available especially when the cracks are subjected to mode III loading. Mode I SIFs can be obtained in open literature however they are also insufficiently completed. Therefore, this paper develops numerically the sickle-shaped crack in round bars using ANSYS finite element program. In order to validate the model, the existing mode I SIFs are used and then compared with the present model. It is found that both models are well agreed with each other. There are two important parameters used such as the crack aspect ratio, a/b and the relative crack depth, a/D ranging between 0.2-1.2 and 0.1-0.6, respectively. SIFs based on J -integral are calculated along the crack fronts for various crack geometries. It is found that the SIFs are significantly affected by a/b and a/D . For the relatively straight-fronted crack ($a/b \leq 0.2$), the SIFs are almost flattened along the crack front. When a/b increased ($a/b > 0.2$), the SIFs have decreased whereas they are increased when a/D increased. It is also found that the SIFs closed to the outer edge are higher than the SIFs at the deepest crack along the crack front. However when $a/b \geq 1.2$, the role of SIFs along the crack fronts are inversed where lower SIFs are observed at the outer point compared with the middle point.

Keywords: *sickle-shape crack; mode III loading; surface crack; round bar.*

Introduction

Shafts in the form of various geometries and shapes are frequently used to transmit power from one point to another. Under certain circumstances, the shafts are exposed to external elements such as corrosion leading to the formation of surface cracks. According to [1], arbitrary initial shape of surface crack grew to take a

semi-elliptical shape. The solutions of SIFs for semi-elliptical crack shapes can be found in [2-4]. However under special conditions, the arbitrary shaped-crack grew to have a sickle-shaped surface cracks. The solutions of SIFs of sickle-shaped cracks can be found in [5-6]. However, the SIFs under mode III loading are not available in open literature.

The sickle-shaped surface cracks occur circumferentially around the solid bar. The fractographic observation can be found in [7]. It is indicated the crack formed around the bolt and propagated into the bar. Once, the crack driving force approached the critical value the bolt experienced the final failure. The finite element analysis on the sickle-shaped crack is documented by Mattheck et al. [7]. However, due to the computational disadvantages, the SIFs of such crack are limited. Based on the comparison between the normalized SIFs among other works, there are huge discrepancies between the results.

Then, Hobbs et al. [8] experimentally conducted using a photoelastic approach on the sickle-shaped cracks. They have concluded that the shape of the crack front does not have a significant effect on the SIFs especially the maximum SIF at the middle of the crack front. However, it does influence the distribution around the crack front. Carpinteri et al. [9] investigated the SIFs of sickle-shaped crack subjected to complex mode I loading. On the other hand, Carpinteri et al. [6] extended their work to study the sickle-shaped crack under eccentric axial loading.

Therefore, this paper presents the solutions of SIFs of sickle-shaped surface cracks in round bars under mode III loading. There are two important parameters that are investigated such as crack aspect ratio, a/b ranging in between 0.2 to 1.2 and relative crack depth, a/D in between 0.1 and 0.6. ANSYS finite element program is used to model and solve the crack problems. The SIFs are then calculated along the crack front of various crack geometries.

Methodology

Sickle-Shaped Cracks

Due to the symmetrical effect only a quarter finite element model is used where the radius, $R = 25$ mm and the half length of the solid round bar is 200 mm. Figure 1 shows the cross-sectional area of sickle-shaped surface crack where O and O' are the central point of circle and semi-ellipse, respectively. The sickle-shaped crack front is based on the semi-elliptic centered at O' . There are seven values of crack aspect or semi-elliptical ratios, a_{minor}/b_{major} used ranging between 0.0 to 1.2 with an increment of 0.2. While, six relative crack depth, a/D are used namely 0.1, 0.2, 0.3, 0.4, 0.5 and 0.6. All of these are used in order to study the influence of different relative crack depths and crack aspect ratios on the stress intensity factors. The SIFs are determined at six different locations along the crack front and the SIF at the point C is not determined due to the singularity problems. It is estimated that the nearest point to point C is 83% measured from point A . The location of each point along the crack front is also normalized such as x/h for the location of point P .

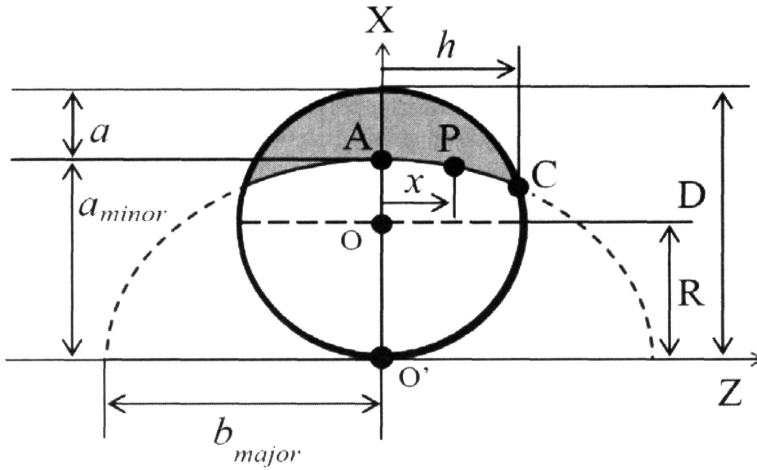


Figure 1: Definition of sickle-shaped crack

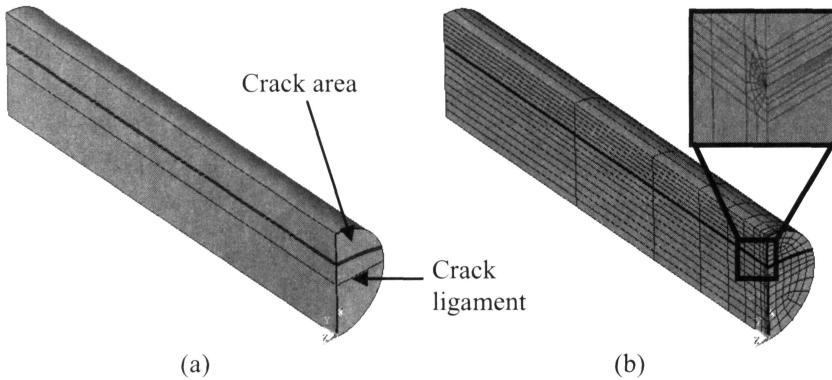


Figure 2: (a) An extruded volume cracked model, (b) Quarter finite element model and its corresponding singular element around the crack tip

Finite Element Modelling

The construction of finite element model is started with the model of cross-sectional area as shown in Figure 2. Once it is completed, the model is extruded along the y-axis with a length of 200 mm. It is selected to ensure the effect of torsion or tension loading is sufficient enough and thus not affecting the stress distribution around the crack region. The extruded volume model is presented in Figure 2(a). Special attention is given at the tip of the sickle-shaped crack where three-dimensional 20-node solid element (SOLID186) is used. The square-root singularity of stresses

and strains around the crack tip is modelled by shifting the mid-point nodes to the quarter-point location close to the tip. Firstly, the two-dimensional model is meshed and then it is swept along the crack front. Then, the remaining model is meshed with irregular similar element. The quarter finite element model is shown in Figure 2(b) with its corresponding crack tip singular element.

In order to remotely apply the bending moment to the model, an independent node is created about 50 mm ahead of bar ends where it is modelled with target element (TARGE170) while the element at the edge of the bar is modelled with node-to-surface contact element (CONTA175). Then, it is required that the whole solid round bar to follow any mechanical movement by the independent node. Then, both the independent node and the nodes at the surface edge of the bar are connected using multiple constraint element (MPC184) as shown in Figure 3. Then, the follower load element (FOLLW201) is used in order to ensure any mechanical displacement occurred at the pilot node to be followed by the solid round bar. On the other hand, the whole edge surface is symmetrically constrained except the crack faces. The left surface plane is also symmetrically constrained. The bending moment is applied to the independent node.

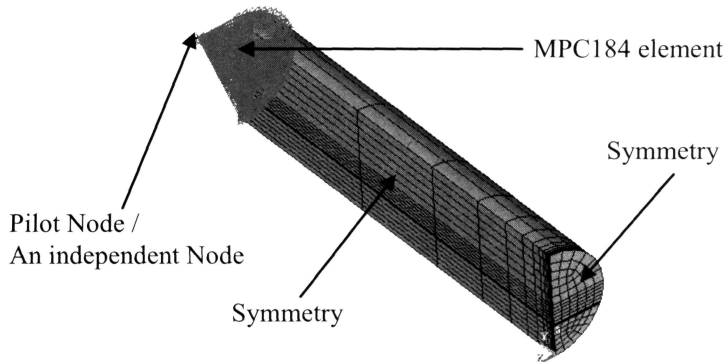


Figure 3: The boundary conditions and the loading on the finite element model

The stress intensity factors (SIF) along the sickle-shape crack front are determined using ANSYS finite element program. The determination of SIFs is based on the J -integral where it can be directly converted into SIFs using Eq. (1) as long as the problem within the elastic ranges and has fulfilled the plain strain condition:

$$K_i = \sqrt{\frac{J_e E}{1-\nu^2}} \quad (1)$$

Where, K_i is a SIF of mode $i = I$ and III, J_e is a J -integral determined directly from program, E is a modulus of elasticity and ν is a Poisson's ratio. In order to generalize the SIFs, it is recommended to convert them into a normalized value called a dimensionless mode I SIF or geometrical correction factor under axial stress, $F_{I,a}$ as Eq. (2):

$$F_{I,a} = \frac{K_{I,a}}{\sigma_a \sqrt{\pi a}} \quad (2)$$

Where, σ_a is a applied bending stress, $K_{I,a}$ is a SIF under axial stress and a is a crack depth. Before the model is further used, it is a compulsory to validate the present model with the existing results of similar finite element model [5]. According to Figure 4, it is revealed that the present model is well agreed with the existing model. Therefore, this present model can be utilized for the further analysis. The model in Figure 3 is only suitable for mode I loading and it cannot be used for mode III loading. Then, it is constructed in full model as shown in Figure 5. At one end, the bar is fully fixed in all degree of freedom while at another end the torsion moment, T is applied at the independent node in order to twist the bar. The dimensionless mode III is normalized according to Eq. (3):

$$F_{III} = \frac{K_{III}}{\tau \sqrt{\pi a}} \quad (3)$$

Where, τ is a applied shear stress, K_{III} is a SIF under shear stress and a is a crack depth.

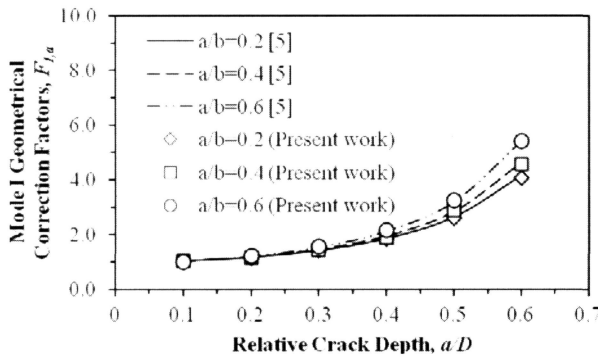


Figure 4: Model validations of the present and the existing models

Results and Discussion

In this paper, the discussion is divided into three categories based on the effect of relative crack depth, a/D , crack aspect ratio, a/b on the SIFs along the crack front and the SIFs at the deepest point ($x/h = 0.0$) along the crack front. Only selected cases of SIFs are discussed since their behaviour are similar but different in magnitudes. The other values of SIFs are tabulated in Table 1.

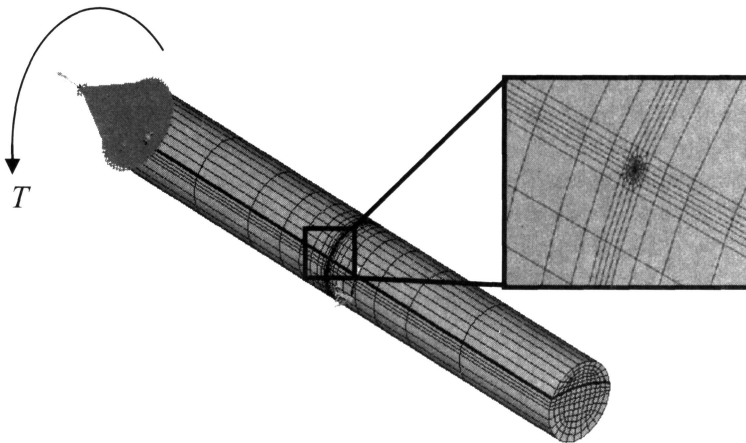


Figure 5: Full finite element model of sickle-shaped surface crack

Effect of Relative Crack Depth on the SIFs

Relative crack depth, $a/D = 0.4, 0.5$ and 0.6 are presented and discussed. Other values of a/D are not presented since the pattern or behaviour of stress intensity factors are almost similar but different in magnitudes. Figure 6 shows the role of relative crack depth on the SIFs along the crack fronts of various crack geometries. It is revealed that the distributions of SIFs are almost similar except when a/D increased, the SIFs are also increased. This behaviour is similar with mode I SIFs as reported in [2]. It is obvious since increasing a/D on the other hand reduced the cross-sectional area of the ligament and therefore increasing the SIFs. The reduction of crack ligament increased the shear stress and therefore affecting the SIFs. Under mode I, for the relatively straight-fronted cracks ($a/b \leq 0.2$), the SIFs along the crack fronts are almost flattened. However under mode III, the role of SIFs are different where the SIFs closed to the outer edge are always higher than the SIFs at the middle point ($x/h = 0.0$). This is due to the fact that at the outer point, the material is easily deformed when compared with the location in the middle along the crack front. Similar SIFs behaviour are observed for other a/b . Once $a/b \geq 1.2$, the SIFs along the crack fronts have changed where the SIFs at $x/h = 0.0$ is slightly

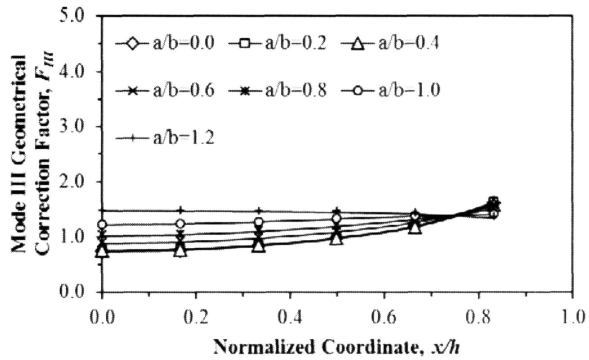
higher than the SIFs at the outer point. It is indicated that once the shape of crack equal to $a/b = 1.2$, the crack growth along the crack front grows in a similar rate and it is initiated at the point $x/h = 0.0$. Whereas for other values of a/b , the crack is first initiated at the area closest to the outer surface.

Effect of Crack Aspect Ratio on the SIFs

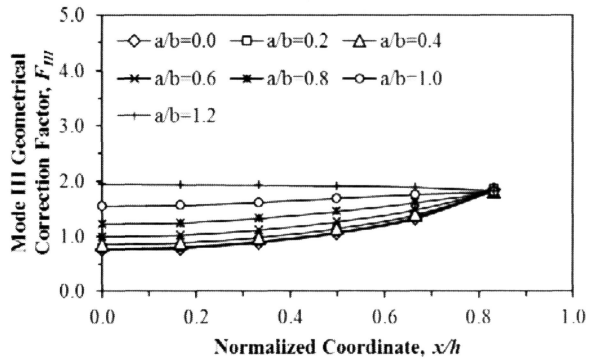
Figure 7 reveals the effect of crack aspect ratio, a/b on the SIFs when the relative crack depth, a/D is varied. In this discussion, $a/b = 0.6, 0.8$ and 1.2 are selected since the role of SIFs along the crack fronts are almost similar except in the magnitude. Figure 7(a) shows the SIFs along the crack front for $a/b = 0.6$ when a/D is varied. It is clearly observed that for the cracks, $a/b \leq 0.4$, the role of SIFs along the crack front is insignificant where changing the crack depth is not greatly affected the SIFs. Similar works on SIFs can be obtained from [2, 3]. The SIFs around the outer surface are slightly higher for higher a/D . Similar SIFs behaviour is observed for $a/b = 0.8$. However the curves of SIFs are flattened. It is indicated that when higher a/b is used, the SIFs around the outer edge are lowered when compared with the SIFs at $x/h = 0.0$. If $a/b = 1.2$ is used, higher SIFs occurred at $x/h = 0.0$. This is due to the fact that when $a/b = 1.2$, the crack formed circumferentially around the cylindrical bar with the maximum crack depth occurred at $x/h = 0.0$. On the other hand, this location also experienced higher shear stress with other points and therefore producing higher SIFs.

SIFs at the Deepest Crack ($x/h = 0.0$)

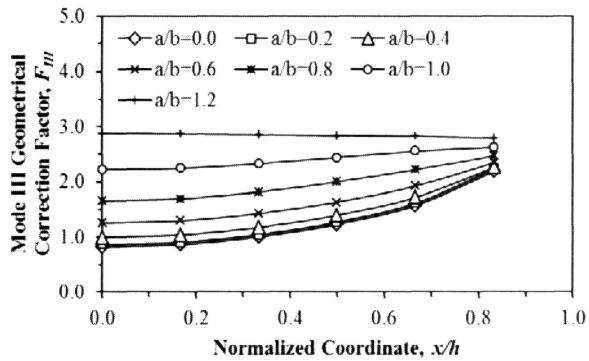
In order to comprehensively understand the SIFs when a/b is varied, it is important to represent the role of SIFs at $x/h = 0.0$ when a/D is increased. This location is important since it is the deepest point along the crack front and also determined the detrimental effect compared with other positions. Figure 8 reveals the SIFs at the deepest point ($x/h = 0.0$) when a/b is varied. It is indicated that the SIFs are significantly dependent on a/D . For $a/b \leq 0.4$, the SIFs are lowered when a/D increased. This is due to the fact that for the relatively straight-fronted crack, higher SIFs occurred at the outer edge and lower SIFs values at the middle point. When higher a/b is used for example $a/b \geq 1.0$, the crack formed circumferentially around the bar and the deepest point occurred at $x/h = 0.0$ and therefore increasing the SIFs. Different behaviour of SIFs are observed for mode I loading [3, 5, 6] where the SIFs at $x/h = 0.0$ are increased as a/D increased. This is due to the different crack opening mechanisms where under mode I loading, the crack faces are always opened across the crack front.



(a)

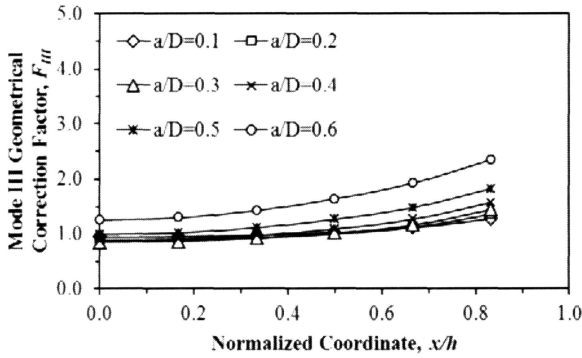


(b)

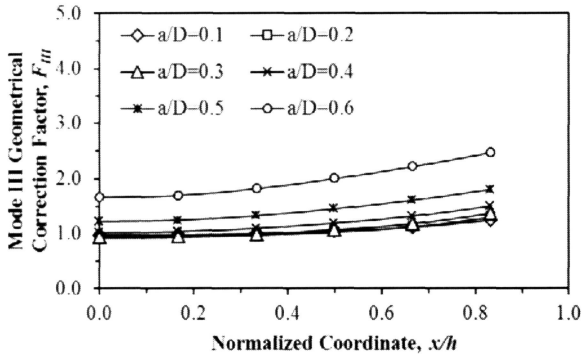


(c)

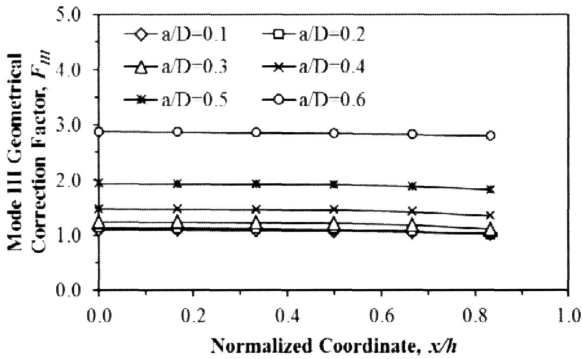
Figure 6: The effect of relative crack depth, a/D on the SIFs when crack aspect ratio, a/b is varied, (a) $a/D = 0.4$, (b) $a/D = 0.5$ and (c) $a/D = 0.6$



(a)



(b)



(c)

Figure 7: The effect of crack aspect ratio, a/b on the SIFs when crack aspect ratio, a/b is varied, (a) $a/b = 0.6$, (b) $a/b = 0.8$ and (c) $a/b = 1.2$

Table 1: List of SIFs of sickle-shaped crack under torsion moments.

x/h	a/D	a/b						
		0.0	0.2	0.4	0.6	0.8	1.0	1.2
0.00	0.1	0.9207	0.9204	0.9349	0.9427	0.9764	1.0297	1.0951
	0.2	0.8206	0.8266	0.8439	0.8787	0.9302	1.0090	1.1252
	0.3	0.7632	0.7734	0.8027	0.8566	0.9408	1.0707	1.2388
	0.4	0.7386	0.7544	0.8013	0.8869	1.0224	1.2241	1.4745
	0.5	0.7525	0.7764	0.8530	0.9956	1.2210	1.5456	1.9349
	0.6	0.8219	0.8635	0.9991	1.2553	1.6601	2.2214	2.8772
0.17	0.1	0.9312	0.9299	0.9441	0.9520	0.9840	1.0355	1.0939
	0.2	0.8341	0.8400	0.8567	0.8907	0.9403	1.0167	1.1226
	0.3	0.7802	0.7908	0.8193	0.8721	0.9542	1.0788	1.2353
	0.4	0.7613	0.7769	0.8229	0.9070	1.0397	1.2345	1.4700
	0.5	0.7822	0.8063	0.8816	1.0227	1.2446	1.5599	1.9276
	0.6	0.8638	0.9051	1.0400	1.2950	1.6956	2.2447	2.8665
0.33	0.1	0.9609	0.9603	0.9738	0.9783	1.0057	1.0534	1.0858
	0.2	0.8793	0.8844	0.8993	0.9295	0.9731	1.0402	1.1134
	0.3	0.8376	0.8495	0.8758	0.9244	0.9982	1.1059	1.2274
	0.4	0.8383	0.8531	0.8966	0.9760	1.0989	1.2731	1.4635
	0.5	0.8839	0.9078	0.9797	1.1152	1.3263	1.6153	1.9209
	0.6	1.0028	1.0444	1.1761	1.4266	1.8165	2.3287	2.8544
0.50	0.1	1.0184	1.0173	1.0268	1.0266	1.0464	1.0869	1.0730
	0.2	0.9616	0.9654	0.9766	0.9998	1.0295	1.0713	1.0964
	0.3	0.9388	0.9541	0.9759	1.0153	1.0716	1.1459	1.2114
	0.4	0.9715	0.9854	1.0230	1.0912	1.1926	1.3261	1.4501
	0.5	1.0551	1.0790	1.1432	1.2654	1.4514	1.6897	1.9084
	0.6	1.2297	1.2721	1.3968	1.6357	1.9979	2.4424	2.8397
0.67	0.1	1.1191	1.1149	1.1203	1.1112	1.1144	1.1415	1.0534
	0.2	1.1039	1.1064	1.1100	1.1195	1.1221	1.1124	1.0670
	0.3	1.1057	1.1296	1.1418	1.1608	1.1805	1.1924	1.1792
	0.4	1.1875	1.1983	1.2237	1.2656	1.3199	1.3797	1.4192
	0.5	1.3222	1.3461	1.3907	1.4804	1.6093	1.7602	1.8817
	0.6	1.5719	1.6158	1.7208	1.9234	2.2195	2.5533	2.8229
0.83	0.1	1.3149	1.3100	1.3047	1.2740	1.2434	1.2417	1.0284
	0.2	1.4006	1.3971	1.3832	1.3562	1.2958	1.1805	1.0089
	0.3	1.4408	1.4923	1.4767	1.4408	1.3644	1.2393	1.1017
	0.4	1.6195	1.6226	1.6083	1.5712	1.4986	1.4110	1.3417
	0.5	1.8295	1.8534	1.8179	1.8207	1.8020	1.8001	1.8210
	0.6	2.1859	2.2301	2.2582	2.3452	2.4690	2.6279	2.7967

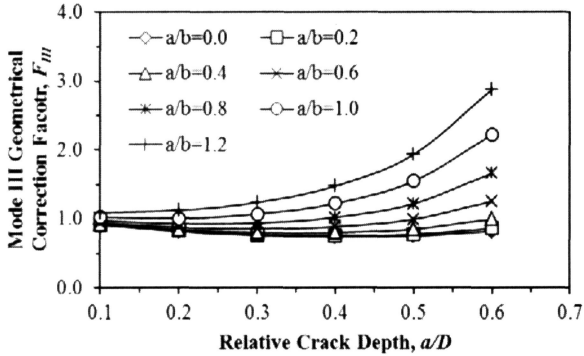


Figure 8: The effect of relative crack depth, a/D when a/b is varied at the deepest point, $x/h = 0.0$

Conclusion

In this paper, sickle-shaped surface crack in round bars are modelled numerically using ANSYS finite element program. Two important parameters are used such as crack aspect ratio, a/b and relative crack depth, a/D and the stress intensity factors are calculated along the crack front, x/h . The model is then subjected to mode III loading from which the following conclusions can be drawn:

1. The SIFs around the outer surface are relatively higher than the SIFs at the middle point. However when $a/b > 1.0$, the maximum SIFs are observed to occur at the middle instead of outer points which is attributed to the change of crack geometries.
2. For the crack geometries of $a/b < 1.0$, the distributions of SIFs are strongly related to the crack front where the SIFs increased at the points closer to the outer surfaces.
3. For the crack geometries of $a/b \geq 1.0$, the maximum SIFs occurred at the deepest points and they decreased along the crack front as it approached the outer points.

References

- [1] X.B. Lin and R.A. Smith, (1999). "Finite element modelling of fatigue crack growth of surface cracked plate, Part II: Crack shape change", *Engineering Fracture Mechanics* 6, 523-540.
- [2] A.E. Ismail, A.K. Ariffin, S. Abdullah and M.J. Ghazali (2012). "Stress intensity factors for surface cracks in round bar under single and combined loadings", *Meccanica* 47(5), 1141-1156.
- [3] J. Toribio, N. Alvarez, B. Gonzalez and J.C. Matos, (2009). "A critical review of stress intensity factor solutions for surface cracks in round bars subjected to tension loading", *Engineering Failure Analysis* 16:794-809.
- [4] A.E. Ismail, A.K. Ariffin, S. Abdullah and M.J. Ghazali, (2012). "Stress intensity factors under combined tension and torsion loadings", *Indian Journal of Engineering and Materials Science* 19:5-16.
- [5] A. Carpinteri, R. Brighenti, S. Vantadori and D. Viappiani, (2006). "Sickle-shaped crack in a round bar under complex mode I loading", *Fatigue and Fracture of Engineering Materials and Structures* 30:524-534.
- [6] A. Carpinteri and S. Vantadori, (2009). "Sickle-shaped surface crack in a notched round bar under cyclic tension and bending", *Fatigue and Fracture of Engineering Materials and Structures* 32:223-232.
- [7] C. Mattheck and Munz D. Morawietz., 1985, "Stress intensity factors of sickle-shaped cracks in cylindrical bars", *International Journal of Fatigue* 7(1):45-47 (1985).
- [8] J. Hobbs, R. Burguete, P. Heyes and E. Patterson, (2001). "A photoelastic analysis of crescent-shaped cracks in bolts", *The Journal of Strain Analysis for Engineering Design* 36(1):93-99.